Concave Hybrid Materials

DOI: 10.1002/ange.201303912

Pd-Cu_2O and Ag-Cu_2O Hybrid Concave Nanomaterials for an Effective Synergistic Catalyst**

*Lingling Li, Xiaobin Chen, Yuen Wu, Dingsheng Wang, Qing Peng, Gang Zhou, and Yadong Li**

Dedicated to Professor Xiao-Zeng You on the occasion of his 80th birthday

Metal–semiconductor or metal–metal-oxide heterostructures have been of great interest for their distinguished properties, such as catalysis,[1] supercapacitor electrodes,[2] and multifunctional probes.[3] A single heterostructure is expected to have a large diversity of shapes, compositions, and especially interfaces, as each of its domains can be tuned, whereby its combinational functionality changes accordingly.[4] For heterostructures, the interface is believed to play a vital role in many cases owing to its distinguished charge state, atomic arrangement, and so on.[5] Rational design of the metal–semiconductor interface might thus help us to obtain catalysts with good activity, selectivity, and/or durability for an idiographic reaction. Admittedly, site-selective growth has provided an efficient way to prepare delicate hybrid architectures with controlled interfaces by regulating one domain to selectively nucleate and grow on specific sites of other domains.[6]

Recently, nanoscale heterostructures were reported to display advantages in organic catalysis, especially as tandem catalysts, owing to their flexibility of structures and compositions.[7] Cu^I compounds are among the leading catalysts in organic reactions, and some are lately introduced into the field of nanocatalysis.[8] Cu_2O is an effective catalyst for oxidative arylation of phenylacetylene,[9] based on which Cu_2O nanocrystal was designated as one domain of the designed heterostructure. Additionally, Lei's group proved that transmetalation is the rate-limiting step in the Sonogashira coupling reaction with palladium complexes and copper(I) as synergistic catalysts by in situ IR spectroscopy.[10] So Pd^0 was chosen as the other domain to test its synergistic effect with Cu_2O in the oxidative arylation of phenylacetylene. To date, several metal–Cu_2O heterostructures have been constructed by wet chemistry routes.[11] However, few Pd-Cu_2O heterostructures were reported, which can possibly be ascribed to the comparative large lattice mismatches between their usually available low-index facets. Great effort needs to be put into developing new heterostructures for Pd-Cu_2O to explore its application as organic catalyst.

We therefore tried to cooperate the two parts with controlled architecture to study its structure-dependent properties. Herein we present a seed-based strategy to construct a site-selective growth of noble metals on Cu_2O nanopolyhedra, the {100} faces of which were more vulnerable than {110} and were gradually oxidatively etched to concaves. Pd NPs and Ag nanodisks preferred different sites of Cu_2O concaves in formation of metal-Cu_2O hybrid concave nanomaterials ("nanoconcaves"). Thereafter, Pd- and Ag-Cu_2O hybrid nanoconcaves were tested and found to have superior catalytic activities to both of the single domains and their mixtures for the Sonogashira-type oxidative arylation of phenylacetylene. This synergistic effect might be the result of electron transfer between metal and Cu_2O, as validated by shifts in XPS spectra and related density functional theory (DFT) calculations, which led to the weakening of interfacial Cu–O bonds and concomitant electron rich of Cu_2O.

Representative Pd-Cu_2O nanocrystals are compiled in Figure 1. Almost a full yield of nanoconcaves was obtained with several NPs of 15 nm on the concavities of Cu_2O octadecahedra. The novel architecture of nanoconcaves was further investigated using its high-magnification SEM and TEM together with high-resolution TEM (HRTEM) images (Figure 1 b,c, and e). The Cu_2O octadecahedron, which is composed of six {100} and twelve {110} facets, was excavated on {100} facets and converted into its concave counterpart.[9] EDX analyses confirmed the existence of Pd (Supporting Information, Figure S2a). Additionally, both mapping and line-scanning indicated the concavity and homogeneous distribution of Pd on the concavities (Figure 1 d; Supporting Information, Figure S2b). However, no metallic Pd could be traced in the XRD data of Pd-Cu_2O hybrid nanoconcaves (Supporting Information, Figure S3), probably on account of the small ratio of Pd in the hybrids that might go beyond the detection limit of the powder diffractormeter. The later ICP-MS data showed the atomic ratio of Pd to Cu was 1.6: 100 (approximately 2.3 wt % of Pd).

The formation process was investigated by sampling at different reaction stages (Supporting Information, Figure S4). Etching of Cu_2O seeds became more severe, as indicated in SEM images and successively weakening of (200) peak in XRD patterns with time. The newly formed Pd^0 atoms

[*] L. L. Li, Y. E. Wu, Dr. D. S. Wang, Dr. Q. Peng, Prof. Y. D. Li
Department of Chemistry, Tsinghua University
Beijing 100084 (China)
E-mail: ydli@mail.tsinghua.edu.cn
X. B. Chen
Department of Physics, Tsinghua University (China)
Prof. G. Zhou
State Key Laboratory of Chemical Resource Engineering, Beijing University of Chemical Technology, Beijing 100029 (China)

[**] This work was supported by the State Key Project of Fundamental Research for Nanoscience and Nanotechnology (2011CB932401 and 2011CBA00500), National key Basic Research Program of China (2012CB224802), and the National Natural Science Foundation of China (Grant No. 21221062, 21171105 and 21131004).

Supporting information for this article is available on the WWW under http://dx.doi.org/10.1002/anie.201303912.

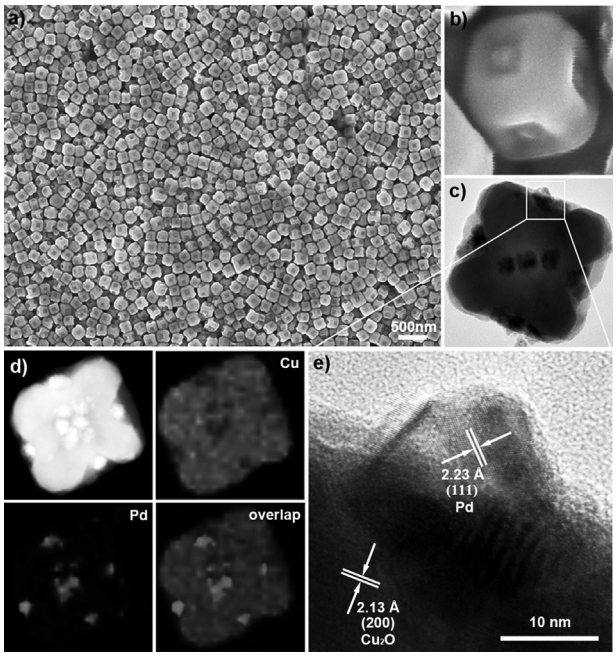

Figure 1. a) SEM image of Pd-Cu_2O nanoconcaves and b) its magnified counterpart; c) high-magnification TEM image and e) HRTEM image recorded in the direction of one concavity of an individual Pd-Cu_2O nanoconcave; d) EDX-mapping with the HAADF-STEM image of the hybrid.

inclined to grow on the concavities driven by thermodynamics since the chemical potential is lower when an atom is added on the concavity than on the flat surfaces.[12] We noticed that noteworthy Pd NPs emerged mainly after the etching of Cu_2O (Supporting Information, Figure S4a,b). $[Pd(OAm)_x]^{2+}$ was supposed to be reduced by the fresh Cu_2O species adjacent to those were just etched,[13] which in turn significantly promoted the etching of Cu_2O octadecahedra. Indeed, the amount of $[Pd(acac)_2]$ had a big impact on the final product of hybrids. Formation of octadecahedral Cu_2O concaves took almost 60 h in absence of $[Pd(acac)_2]$ (Supporting Information, Figure S5 and Figure S6a–d). When plentiful $[Pd(acac)_2]$ was supplied, the vast majority of Cu_2O seeds were excessively etched in formation of 4 nm sized tetrahedral Pd NPs. Pd NPs were overgrown into dendrites after 9 h (Supporting Information, Figure S6). As such, $[Pd(acac)_2]$ was believed to have accelerated the etching of Cu_2O octadecahedra, but not as a catalyst as was previously reported.[14]

The composition and morphology of the final product were demonstrated to be strictly affected by reaction conditions. No depression could be perceived on any faces after 60 h under Ar purge, and Pd NPs scattered randomly around flat faces of Cu_2O. When the reaction system was aerated with an O_2 balloon (ca. 500 mL of pure O_2), Cu_2O octadecahedra were pronouncedly pitted on {100} faces after 12 h, and later subject to severe corrosion at 24 h (Supporting Information, Figure S7). The above results strongly identified the etching of Cu_2O was an O_2-participated oxidative reaction. Some previous reports found {100} were the most stable faces.[15] We speculated that the absorption capability of OAm might vary on different facets of Cu_2O seeds, and consequently affected the binding sites for O_2. Such facet-selective capping has been previously reported.[12] This speculation was later verified (Supporting Information, Figure S8). In absence of OAm, Cu_2O octadecahedra were etched mainly on corners and edges in low coordination states. This preliminarily demonstrated that OAm could promote the selective corrosion of {100}. Herein, reducibility and Pd precursor also played important roles in controlling the reaction kinetics and finally the products. We tried elevating the reducibility of the system to reduce dimensions of Pd in the Pd-Cu_2O nanoconcave by introducing borane–tert-butylamine complex (TBAB, 0.01 mmol) as a strong reductant. Pd NPs were obtained scattering off Cu_2O with much smaller sizes (Supporting Information, Figure S9). $[Pd(OAm)_x]^{2+}$ stripped electrons from TBAB rather than Cu^+ species, and thus they were unable to grow on Cu_2O. $Pd(OAc)_2$ provided similar structure to $[Pd(acac)_2]$ as OAc^- and $acac^-$ are both bidentate ligands. For $PdCl_2$, Cu_2O were completely etched within 36 h, presumably promoted by the Cl^-/O_2 etching (Supporting Information, Figure S10).[16]

We further demonstrated this strategy was applicable for Ag-Cu_2O hybrid nanoconcaves. Though flat Cu_2O octadecahedra were also subject to etching and converted into their concave counterparts, the growth of Ag was distinct from that of Pd. As shown in Figure 2, Ag NPs had a disk-like shape,

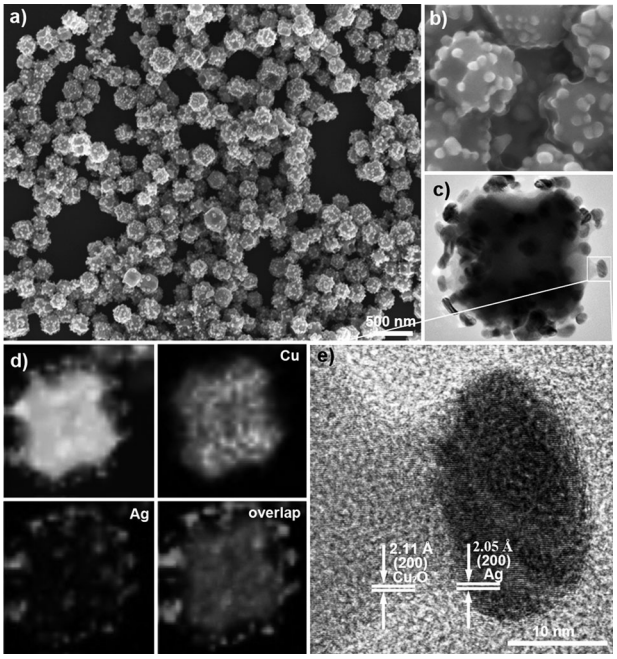

Figure 2. a) SEM image of Ag-Cu_2O nanoconcaves and b) its magnified counterpart; c) high-magnification TEM image and e) HRTEM image of an edge of an individual Ag-Cu_2O nanoconcave; d) EDX-mapping with the HAADF-STEM image.

and their average diameter and height were measured as $D = 23$ nm and $h = 10$ nm, respectively. Ag nanodisks had a propensity to grow on edges and vertices of Cu_2O nanoconcaves (Figure 2 a–c). As depicted in Figure 2 e, Ag^0 directly inter-

faced with Cu_2O through epitaxial growth owing to their moderate lattice mismatch of {200} faces (4.2%). The two discrete sets of XRD patterns of Ag-Cu_2O could be separately indexed to cubic Ag and Cu_2O (Supporting Information, Figure S3). Ag was also confirmed by EDX analyses (Figure 2d; Supporting Information, Figure S11). Based on ICP-MS analysis, the amount of Ag reached up to 9 mol% (Ag/Cu = 4.9:100 in mole) in the hybrid nanoconcaves.

In terms of Ag-Cu_2O nanoconcaves, Ag^+ could also be reduced by Cu_2O according to the different electrochemical redox potentials.[13] In the present system, a mass of Ag NPs formed immediately when the temperature reached 120°C, indicating the reduction of $[Ag(OAm)_x]^+$ was much easier than $[Pd(OAm)_x]^+$ by Cu^+ species (Supporting Information, Figure S12a). Consequently, Ag^0 nucleated preferentially at edges and vertices of Cu_2O seeds which were shown to be more active than faces,[17] together with a small fraction on {100} faces at the initial stage. Then more Ag grew with the ⟨100⟩ orientation in formation of disks (Supporting Information, Figure S12b,c). Afterwards, with the unceasing oxidative etching of Cu_2O on its {100} facets by O_2, most Ag nanodisks were finally on the edges and vertices of concave Cu_2O, and phase evolution was revealed (Supporting Information, Figure S12).Accordingly, the proposed formation of Cu_2O, Pd-Cu_2O and Ag-Cu_2O nanoconcaves is illustrated in the Supporting Information, Figure S13.

In our previous work, Cu_2O octadecahedra provided good activity in the aerobic oxidative arylation of phenylacetylene.[9] This reaction was herein introduced to test properties of Pd-Cu_2O and Ag-Cu_2O hybrid nanoconcaves (Supporting Information, Scheme S1). Pd/Ag-Cu_2O provided excellent yields of 95% and 91% after 20 h, and their time-dependent catalytic activity is shown in the Supporting Information, Table S1. As the common domain of the hybrids, Cu_2O nanoconcaves were less active in ca. 72% yield (Supporting Information, Table S2, entry 1). So it is supposed that the enhanced activity of hybrids might have association with Pd and Ag counterparts. Pd NPs/C and commercial Pd/C were inactive in the reaction during the whole process, while the activity of Ag nanodisks and Ag NPs/C began to be detectable by 12 h in 37% and 41% yields (Supporting Information, Figure S14; Table S2, entries 2, 3, and 6). Besides, Pd NPs/C + Cu_2O nanoconcaves and Ag nanodisks + Cu_2O nanoconcaves were less active compared with their hybrid counterparts (Supporting Information, Table S2, entries 4 and 5). The integrate comparisons of activities among the catalysts were illustrated in Figure 3. The hybrids had a higher rate than Cu_2O at the initial stage of the catalysis (Supporting Information, Figure S15). After catalysis, the structure and composition were basically maintained for Pd/Ag-Cu_2O hybrid nanoconcave, and no evident oxidation was observed (Supporting Information, Figure S16–18). The hybrids could be recycled without noteworthy decrease of activity, 92% for Pd-Cu_2O and 89% for Ag-Cu_2O after 20 h in the second run. Afterwards the hot filtration was performed, which is one of the valid heterogeneity tests.[18] GC showed filtrate 1 and 2 proceeded to 45% and 41% respectively for a total time of 20 h, hardly any increase in yield compared with 41% at 1 h (see the Supporting Information). Notably, in present catalysis, phenylboronic acid was adopted as the substrate instead of the commonly used aryl halides, and thus Pd NPs could be prevented from leaching.[19]

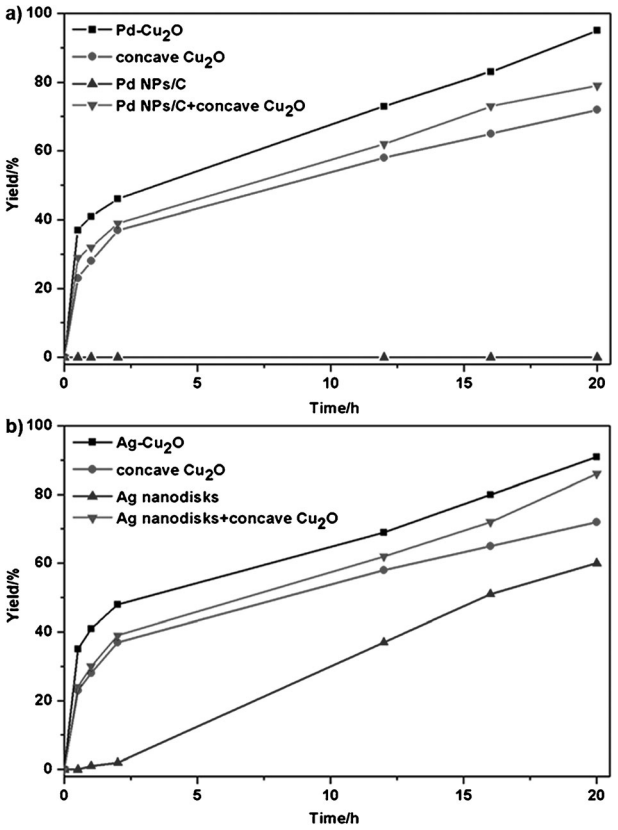

Figure 3. Catalytic activities as a function of time in the model reaction for catalysts: a) Pd-Cu_2O hybrid nanoconcave, the single domains (Pd NPs/C, concave Cu_2O) and its mixtures as Pd NPs/C + concave Cu_2O; b) Ag-Cu_2O hybrid nanoconcave, the single domains (Ag nanodisks, concave Cu_2O) and its mixtures as Ag nanodisks + concave Cu_2O.

We referred to X-ray photoelectron spectroscopy (XPS) to inspect the interaction between noble metals and the host, because coupling will cause changes of spectroscopic properties of the hybrid.[20] As shown in Figure 4a, the peaks at 932.7 and 952.5 eV could be assigned to Cu $2p_{3/2}$ and Cu $2p_{1/2}$ of Cu_2O nanoconcaves with binding energy calibrated with C 1s = 284.8 eV. XPS spectrum of Pd-Cu_2O hybrids depicted that the binding energy of Cu $2p_{3/2}$ decreased by 0.2 eV relative to that of Cu_2O nanoconcaves. Moreover, the binding energies of Pd and Ag in hybrid nanoconcaves were slightly shifted up when compared with their single domains as Pd NPs and Ag nanodisks (Supporting Information, Figure S19 and 20). The above shifts could probably be ascribed to electron transfer from the noble metal domain to Cu_2O host.[20b,c]

To elucidate, the nature of synergistic effects in the Pd/Ag-Cu_2O nanoconcaves, we performed extensive theoretical investigations using DFT. The calculated work functions of Pd and Ag were smaller than that of {100} faces of Cu_2O with the O-terminated surface (7.27 eV) which was regarded as the normal state (Supporting Information, Table S3).[21] This

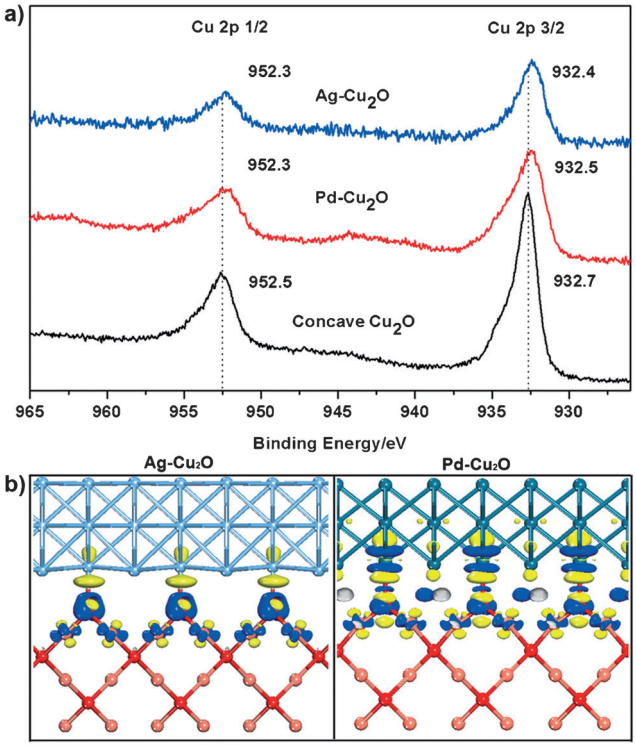

Figure 4. a) Cu 2p XPS spectra of Pd-Cu_2O, Ag-Cu_2O, and Cu_2O nanoconcaves. b) Difference charge density in Ag-Cu_2O (left) and Pd-Cu_2O (right) nanoconcaves with the Ag/O- and Pd/O-terminal interfaces, respectively, referred from the experimental observations. Blue and yellow areas represent the charge accumulation and depletion, respectively. The isosurface value is 0.03 e Å^{-3}. O Red, Cu brick-red, Ag light blue, Pd cyan.

indicated the possibility of charge transfer between two domains of the hybrids. The electron transfer associated with metal–oxide interactions was irrespective of the morphologies of metal and oxide,[22] so we proposed a straightforward interface model for the hybrid nanoconcaves to directly track the charge transfer in the interface region, and analyzed its effects on the interface property from and the domains from electronic contributions. In what follows, the Ag-Cu_2O hybrid nanoconcave was taken as an example because its epitaxial growth on {100} of Cu_2O was clearly observed (Figure 2e). More precisely, difference charge density (Figure 4b) and Bader charge analysis showed that in addition to the electron transfer from Pd/Ag to Cu_2O (0.25/0.36e), part of donated electrons of interfacial O were steady transferred back to the neighboring Cu^+ (0.17/0.2e), indicating an electronic compensation mechanism of metal oxides. This process made the interfacial Cu–O bonds weak (Figure 4b), thereby facilitating activated oxygen transfer from metal oxide to Pd/Ag; and led to partial oxidation of Pd/Ag and concomitant partial reduction of Cu_2O. These two consequences might help to enhance the catalytic activity of hybrid nanoconcaves, resembling Pt-ceria nanocatalysts.[22]

Further evidence for such the electron transfer in hybrids was UV/Vis spectra. As expected, the donated electrons from Ag would suppress the presence of holes or combine with the holes in Cu_2O, which is a p-type semiconductor in nature. As a result, the band gap of Ag-Cu_2O nanoconcaves increased, corresponding to the blue-shifted peak of UV/Vis spectrum relative to Cu_2O nanoconcaves, which is consistent with the measured UV/Vis spectra (Supporting Information, Figure S21). It was the same case for Pd-Cu_2O hybrids. Lei showed that transmetalation of the Sonogashira reaction is the rate-limiting step by in situ IR spectroscopy.[10] The electron-rich alkyne–copper species with enhanced nucleophilicity would facilitate the transmetalation reaction with Pd intermediate and further the whole reaction. As a result, Pd-Cu_2O hybrid nanoconcaves showed superior catalytic activities to their mixture of single domains in the Sonogashira-type reaction. It should be noted that Ag cannot participate the oxidative addition and reductive elimination reaction as Pd did, and thus should not keep to such a catalytic cycle. The specific relationship of charge transfer with enhanced catalytic properties for Ag-Cu_2O hybrid nanoconcaves is now under investigation.

In summary, Pd NP-Cu_2O and Ag nanodisk-Cu_2O hybrid nanoconcaves were prepared through site-selective growth of noble metals on Cu_2O seeds. Pd could only nucleate on the cavities of Cu_2O, while Ag^0 principally grew on edges and vertices of concave Cu_2O. The hybrid nanoconcaves exhibited superior catalytic activities to the single domains and their mixtures for the model organic reaction. Shifts of Cu 2p and Pd (or Ag) 3d in the XPS spectra of the hybrids, together with DFT results, preliminarily revealed the electron transfer from the noble metal part to the Cu_2O host, which could be the cause of synergistic effect of the hybrid nanonconcaves. From the synergistic effects, correlated with the electronic compensation mechanism of metal oxides, we could propose the similar metal/oxide heterostructures as a potential candidate for a catalyst if following the two fundamental principles: 1) a good lattice match between metal and oxide, ensuring potential metal–oxide interaction; and 2) a pronounced work function difference, corresponding to a steady electron transfer between domains.

Received: May 7, 2013
Revised: July 3, 2013
Published online: August 26, 2013

Keywords: concave nanohybrids · density functional calculations · heterogeneous catalysis · site-selective growth · synergistic effects

[1] a) A. Bruix, J. A. Rodriguez, P. J. Ramírez, S. D. Senanayake, J. Evans, J. B. Park, D. Stacchiola, P. Liu, J. Hrbek, F. Illas, *J. Am. Chem. Soc.* **2012**, *134*, 8968; b) C. Wang, H. Yin, S. Dai, S. Sun, *Chem. Mater.* **2010**, *22*, 3277; c) B. Wu, H. Zhang, C. Chen, S. Lin, N. Zheng, *Nano Res.* **2009**, *2*, 975; d) F. Liao, Z. Zeng, C. Eley, Q. Lu, X. Hong, S. C. E. Tsang, *Angew. Chem.* **2012**, *124*, 5934; *Angew. Chem. Int. Ed.* **2012**, *51*, 5832.

[2] Q. Lu, M. W. Lattanzi, Y. Chen, X. Kou, W. Li, X. Fan, K. M. Unruh, J. G. Chen, J. Q. Xiao, *Angew. Chem.* **2011**, *123*, 6979; *Angew. Chem. Int. Ed.* **2011**, *50*, 6847.

[3] a) C. Xu, J. Xie, D. Ho, C. Wang, N. Kohler, E. G. Walsh, J. R. Morgan, Y. E. Chin, S. Sun, *Angew. Chem.* **2008**, *120*, 179; *Angew. Chem. Int. Ed.* **2008**, *47*, 173; b) S.-H. Choi, H. B. Na, Y. I. Park, K. An, S. G. Kwon, Y. Jang, M.-H. Park, J. Moon, J. S.

Son, I. C. Song, W. K. Moon, T. Hyeon, *J. Am. Chem. Soc.* **2008**, *130*, 15573.
[4] a) J. B. Park, J. Graciani, J. Evans, D. Stacchiola, S. D. Senanayake, L. Barrio, P. Liu, J. F. Sanz, J. Hrbek, J. A. Rodriguez, *J. Am. Chem. Soc.* **2010**, *132*, 356; b) M. R. Buck, J. F. Bondi, R. E. Schaak, *Nat. Chem.* **2012**, *4*, 37.
[5] a) M. Haruta, *CATTECH* **2002**, *6*, 102 – 115; b) U. Landman, B. Yoon, C. Zhang, U. Heiz, M. Arenz, *Top. Catal.* **2007**, *44*, 145; c) Q. Fu, W.-X. Li, Y. Yao, H. Liu, H.-Y. Su, D. Ma, X.-K. Gu, L. Chen, Z. Wang, H. Zhang, B. Wang, X. Bao, *Science* **2010**, *328*, 1141; d) J. Zhang, Q. Xu, Z. Feng, M. Li, C. Li, *Angew. Chem.* **2008**, *120*, 1790; *Angew. Chem. Int. Ed.* **2008**, *47*, 1766.
[6] a) C. Gao, Q. Zhang, Z. Lu, Y. Yin, *J. Am. Chem. Soc.* **2011**, *133*, 19706; b) F.-R. Fan, Y. Ding, D.-Y. Liu, Z.-Q. Tian, Z. L. Wang, *J. Am. Chem. Soc.* **2009**, *131*, 12036; c) P. Li, Z. Wei, T. Wu, Q. Peng, Y. Li, *J. Am. Chem. Soc.* **2011**, *133*, 5660.
[7] a) T. Yu, J. Zeng, B. Lim, Y. Xia, *Adv. Mater.* **2010**, *22*, 5188; b) K. V. S. Ranganath, J. Kloesges, A. H. Schäfer, F. Glorius, *Angew. Chem.* **2010**, *122*, 7952; *Angew. Chem. Int. Ed.* **2010**, *49*, 7786; c) Y. Yamada, C.-K. Tsung, W. Huang, Z. Huo, S. E. Habas, T. Soejima, C. E. Aliaga, G. A. Somorjai, P. Yang, *Nat. Chem.* **2011**, *3*, 372.
[8] N. Krause, A. Hoffmann-Röder, *Modern Organocopper Chemistry*, Wiley-VCH, Weinheim, **2002**.
[9] L. Li, C. Nan, Q. Peng, Y. Li, *Chem. Eur. J.* **2012**, *18*, 10491.
[10] C. He, J. Ke, H. Xu, A. Lei, *Angew. Chem.* **2013**, *125*, 1567; *Angew. Chem. Int. Ed.* **2013**, *52*, 1527.
[11] a) C.-H. Kuo, T.-E. Hua, M. H. Huang, *J. Am. Chem. Soc.* **2009**, *131*, 17871; b) J. Zeng, J. Huang, C. Liu, C. H. Wu, Y. Lin, X. Wang, S. Zhang, J. Hou, Y. Xia, *Adv. Mater.* **2010**, *22*, 1936; c) L. Zhang, D. A. Blom, H. Wang, *Chem. Mater.* **2011**, *23*, 4587; d) L. Pan, L. Li, Y. Chen, *Micro Nano Lett.* **2011**, *6*, 1019; e) L. Kong, W. Chen, D. Ma, Y. Yang, S. Liu, S. Huang, *J. Mater. Chem.* **2012**, *22*, 719; f) Y. Pan, S. Deng, L. Polavarapu, N. Gao, P. Yuan, C. H. Sow, Q.-H. Xu, *Langmuir* **2012**, *28*, 12304; g) Z. Wang, S. Zhao, S. Zhu, Y. Sun, M. Fang, *CrystEngComm* **2011**, *13*, 2262.
[12] H. Zhang, M. Jin, Y. Xia, *Angew. Chem.* **2012**, *124*, 7774; *Angew. Chem. Int. Ed.* **2012**, *51*, 7656.
[13] A. J. Bard, R. Parsons, J. Jordan, *Standard Potentials in Aqueous Solution*, Marcel Dekker, New York, **1985**.
[14] C. Lu, L. Qi, J. Yang, X. Wang, D. Zhang, J. Xie, J. Ma, *Adv. Mater.* **2005**, *17*, 2562.
[15] a) C. H. Kuo, C. H. Chen, M. H. Huang, *Adv. Funct. Mater.* **2007**, *17*, 3773; b) Y. M. Sui, W. Y. Fu, Y. Zeng, H. B. Yang, Y. Y. Zhang, H. Chen, Y. X. Li, M. H. Li, G. T. Zou, *Angew. Chem.* **2010**, *122*, 4378; *Angew. Chem. Int. Ed.* **2010**, *49*, 4282; c) H. Bao, W. Zhang, D. Shang, Q. Hua, Y. Ma, Z. Jiang, J. Yang, W. Huang, *J. Phys. Chem. C* **2010**, *114*, 6676.
[16] Y. Xiong, J. Chen, B. Wiley, Y. Xia, S. Aloni, Y. Yin, *J. Am. Chem. Soc.* **2005**, *127*, 7332.
[17] Y. Wu, D. Wang, Z. Niu, P. Chen, G. Zhou, Y. Li, *Angew. Chem.* **2012**, *124*, 12692; *Angew. Chem. Int. Ed.* **2012**, *51*, 12524.
[18] R. A. Sheldon, M. Wallau, I. W. C. E. Arends, U. Schuchardt, *Acc. Chem. Res.* **1998**, *31*, 485.
[19] a) M. Portnoy, D. Milstein, *Organometallics* **1993**, *12*, 1665; b) N. T. S. Phan, M. Van Der Sluys, C. W. Jones, *Adv. Synth. Catal.* **2006**, *348*, 609; c) R. Chinchilla, C. Nájera, *Chem. Rev.* **2007**, *107*, 874; d) Z. Niu, Q. Peng, Z. Zhuang, W. He, Y. Li, *Chem. Eur. J.* **2012**, *18*, 9813.
[20] a) M. Pang, J. Hu, H. C. Zeng, *J. Am. Chem. Soc.* **2010**, *132*, 10771; b) Z. Jiang, W. Zhang, L. Jin, X. Yang, F. Xu, J. Zhu, W. Huang, *J. Phys. Chem. C* **2007**, *111*, 12434; c) J. Yang, J. Y. Ying, *Angew. Chem.* **2011**, *123*, 4733; *Angew. Chem. Int. Ed.* **2011**, *50*, 4637.
[21] a) K. H. Schulz, D. F. Cox, *Phys. Rev. B* **1991**, *43*, 1610; b) D. Le, S. Stolbov, T. S. Rahman, *Surf. Sci.* **2009**, *603*, 1637.
[22] G. N. Vayssilov, Y. Lykhach, A. Migani, T. Staudt, G. P. Petrova, N. Tsud, T. Skála, A. Bruix, F. Illas, K. C. Prince, V. R. Matolín, K. M. Neyman, J. Libuda, *Nat. Mater.* **2011**, *10*, 310.

